Magnetic property of a staggered-array undulator using a bulk high-temperature superconductor

Ryota Kinjo,* Kenta Mishima, Yong-Woon Choi, Mohamed Omer, Kyohei Yoshida, Hani Negm, Konstantin Torgasin, Marie Shibata, Kyohei Shimahashi, Hidekazu Imon, Kensuke Okumura, Motoharu Inukai, Heishun Zen, Toshiteru Kii, Kai Masuda, Kazunobu Nagasaki, and Hideaki Ohgaki

Institute of Advanced Energy, Kyoto University, Gokasho, Uji, Kyoto 611-0011, Japan

(Received 11 September 2013; published 26 February 2014)

The magnetic field of a staggered-array undulator using a bulk high-temperature superconductor is calculated by analytical and numerical methods. Analytical formulas for the undulator field and the solenoid field required to generate the undulator field are derived from a simple two-dimensional model. The analytical calculation shows the degree of dependence of these fields on the undulator parameters, the generation of a high undulator field proportional to the critical current density of the bulk superconductor, and the good tunability of the undulator field over a wide range of values. The numerical calculation is performed in a three-dimensional geometry by two methods: the center field and energy minimization methods. The latter treats the current distribution inside the bulk, whereas the former neglects it as a natural extension of the analytical model. The calculation also reveals the dependence of the fields on the undulator parameters arising from the current distribution. From the comparison with experimental results, we find that the latter method reproduces the experimental results well, which indicates the importance of the current distribution inside the bulk. Therefore, we derive a semiempirical formula for the required solenoid field by modifying the analytical formula using the numerical results so as to include the effect of the current distribution. The semiempirical formula reproduces the numerical result with an error of 3%. Finally, we estimate the magnetic performance of the undulator as an example of using the formulas and values presented in this paper. The estimation shows that an undulator field twice as large as that of the present in-vacuum undulator but with an equal period and gap can be obtained at a temperature of approximately 20–40 K, and that deflection parameters (K values) of 1 and 2 can be achieved with periods of 5 and 10 mm at approximately 4–20 K.

DOI: 10.1103/PhysRevSTAB.17.022401 PACS numbers: 07.85.Qe

I. INTRODUCTION

Synchrotron radiation from a relativistic electron beam passing through an undulator, i.e., undulator radiation, and free electron lasers (FELs) are crucial to a wide range of scientific applications. The fundamental wavelength of undulator radiation and FELs depends on the electron beam energy E, undulator period λ_u, and undulator field strength B_0. As undulators had typically had periods of cm order, the only way to obtain bright undulator radiation in the hard x-ray region (10–25 keV) had been to use high-energy electron beams in large synchrotron facilities such as the European Synchrotron Radiation Facility in France ($E = 6$ GeV), Advanced Photon Source in the U.S. (7 GeV), and SPring-8 in Japan (8 GeV). A demonstration of 4.6 keV x-ray generation from the 2.584 GeV synchrotron in the National Synchrotron Light Source was performed with an 11-mm-period undulator [1]. Since then, moderate-energy synchrotron facilities with short-period undulators, such as the Swiss Light Source in Switzerland ($E = 2.4$ GeV, $\lambda_u = 17$ mm), DIAMOND in the U.K. (3 GeV, 21 mm), and SOLEIL in France (2.75 GeV, 20 mm), have been constructed [2–4]. In these facilities, the fundamental wavelengths of undulator radiation reach the x-ray region; harmonics from the 5th through 11th reach the hard x-ray region. This scheme also prevails for FELs. The first x-ray laser of 0.12 nm (10 keV) was achieved at LCLS in the U.S. (15 GeV, 30 mm) [5], and such lasers have already been used for x-ray science [6]. Subsequently, a 0.06 nm (20 keV) FEL was achieved at SACLA in Japan (8 GeV, 18 mm) [7]. Recently, an x-ray FEL using the 3rd and 5th harmonics from a 3 GeV electron beam source and a 15-mm-period undulator has been proposed [8]. As can be concluded from the above, short-period undulators require lower electron beam energies, meaning lower costs, a shorter construction time, and

*r-kinjo@spring8.or.jp
Present address: RIKEN SPring-8 Center, 1-1-1, Kouto, Sayo-Cho, Sayo-Gun, Hyogo 679-5148, Japan.

less effort, and also provide opportunities for scientists to use hard x rays in various applications. The undulator field strength, although not a determining parameter for the wavelength, must be sufficiently high to maintain the brilliance of the radiation, especially that of the harmonics, and the gain of amplification in FELs at a high level with a short-period undulator and low-energy electron beam. In addition, the use of multi-MeV gamma rays from high-field, short-period undulators to generate polarized positron beams via particle-antiparticle pair production in future linear colliders has been proposed [9].

To realize higher-field, shorter-period undulators, several different types of undulator have been studied. In-vacuum undulators (IVUs) [10], which have specially coated permanent magnet (PM) arrays inside a vacuum vessel, have been used in the aforementioned demonstration and in moderate-energy facilities. Cryogenic PM undulators (CPMUs) [11], in which the residual flux and coercivity of PMs are enhanced by cooling the magnets in an IVU to 100–150 K, have been developed and put in use. An undulator using a low-temperature superconductor (LTS), generally called a superconducting undulator before high-temperature superconductor (HTS) undulators were invented, has come under review. The insertion of LTS wires in a vacuum vessel has been proposed and demonstrated by Hezel *et al.* [12], who attempted to remove the thick wall of thermal insulation between the electron beam trajectory and the LTS wires.

Recently, bulk HTSs have been extensively studied; a trapped field of over 17 T was reported in a 26-mm-diameter, 15-mm-thick bulk HTS at 29 K [13]. An undulator using a bulk HTS has several advantages over other undulators: (1) a bulk HTS can produce fields over 10 times stronger than those of PMs even when the PMs are cooled; (2) the magnetic properties of bulk HTSs are continuing to improve, whereas those of PMs have reached a limit; (3) HTSs are more suitable than LTSs in high-current accelerators, in which the thermal input from the electron beam and the radiation itself is high; (4) assembly is easier than for an undulator using LTSs. However, to use bulk HTSs in undulators, one has to investigate methods of magnetizing bulk HTSs and generating a sinusoidal magnetic field, i.e., an undulator field. So far, various approaches to achieving this have been proposed. Cryoundulator plus (CU+) [14], in which bulk HTS rings are mounted on PMs to enhance the magnetic field in a CPMU, has been proposed and demonstrated. A superconducting PM undulator [15,16], in which bulk HTSs are magnetized by a dipole field perpendicular to the beam axis, has also been developed.

We previously proposed and developed a bulk HTS staggered array undulator (BHSAU) [17], a schematic diagram of which is shown in Fig. 1. The principle of operation is as follows. When a solenoid field is applied to the bulk HTSs in the negative-z direction, superconducting current loops are established to negate the change in the magnetic field inside the bulk HTSs; therefore, the bulk HTSs are magnetized in the positive-z direction and thus generate a sinusoidal magnetic field in the y direction. The BHSAU is based on a conventional staggered-array undulator (SAU) [18], in which soft magnetic blocks are in a staggered-array configuration instead of bulk HTSs. Therefore, the BHSAU inherits the properties of an SAU, i.e., tunability of the undulator field by the solenoid field. The advantages of the BHSAU are as follows. Because the undulator field is generated by bulk HTSs, which are magnetized in the same direction, one external solenoid can magnetize all the bulk HTSs and control the undulator field by controlling the magnetization of the bulk HTSs. Thus, a mechanical structure to control the gap is not required. Considering the large attraction force in a high-field undulator and the fact that cracking of the bulk HTSs occurred in the demonstration experiment of CU+, this is a major advantage. So far, the demonstration of high-field generation at 6 K has been performed. An undulator field of $B_0 = 0.85$ T was achieved at 6 K in a 6-periodic-number, 10-mm-period, 4-mm-gap prototype with a 2 T superconducting solenoid and a helium gas cooling system [19]. In the demonstration, we could only use a 2 T solenoid and rather small bulk HTSs because of budgetary restrictions. Even stronger undulators can be expected using a stronger solenoid.

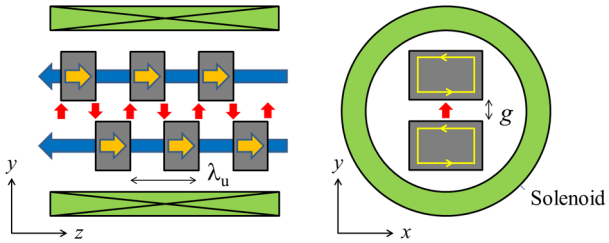

FIG. 1. Schematic view of BHSAU.

Owing to a lack of formulas or computation codes to reproduce the undulator field of the BHSAU, the characteristics of the field inside the BHSAU have not been well studied. For a conventional PM undulator, the Halbach formula [20] can be used to easily estimate the undulator field. A three-dimensional magnetic field computation code, RADIA [21], which was developed in ESRF Insertion Device Laboratory, is commonly used to design undulators using PMs, ferromagnetic pieces, and/or electromagnetic coils. For an undulator using bulk HTSs, conventional methods cannot be used because of the difficulty of calculating the magnetization of a bulk HTS. The superconducting loop current inside a bulk HTS depends on the critical current density J_c, the current distribution, and the history of the applied field after the superconducting transition. To further complicate matters, J_c at a certain point in a bulk HTS depends on the magnetic field at the point. For example, values of J_c for a small

TABLE I. Critical current density of QMG-GdBCO under magnetic field. Measurements were carried out by the dc magnetization method with a small sample (~0.2 mm^3).

T [K] ($T_c = 94$ K)	J_c [kA/mm^2] $B = 0$ T	2 T	4 T	6 T
4	24	18	13	12
10	16	11	8.7	8.2
20	9.4	5.4	5.3	5.3
40	3.5	2.2	2.4	2.2
60	1.5	0.86	0.60	···

sample of QMG-GdBCO measured by the dc magnetization method are listed in Table I. Here, QMG-GdBCO from Nippon Steel Corporation [22] was the bulk HTS used in the experiment. To calculate the magnetization of bulk HTSs, there are multiple steps depending on the required accuracy. The first step is to use a simple current distribution that does not vary in the z direction and a constant J_c corresponding to the average critical current density in all bulk HTSs. The second is to use a current distribution that varies in the z direction and a constant J_c. The third is to use a current distribution that varies in the z direction and a J_c that depends on the field.

In this paper, the magnetic properties of the BHSAU are studied. We develop an analytical model and derive analytical formulas for the undulator field and the solenoid field required to generate the undulator field. A constant J_c and a simple current distribution are assumed. The basic characteristics of the fields are obtained using the formulas. Moreover, we develop a three-dimensional numerical model to precisely calculate these fields. The numerical computation is performed by two methods to investigate the effect of the current distribution. One method is to assume a simple current distribution, and the other method is to treat the z-direction distribution of the current. A comparison with experimental results is also made to evaluate the methods. To precisely estimate the fields without a large computation cost, a semiempirical formula for the solenoid field is derived from the analytical formulas using the result of comparing the analytical and numerical calculations. Finally, we estimate the magnetic performance of the undulator as an example of using the formulas.

II. METHOD

A. Analytical calculation

Here, we discuss the simple two-dimensional model used for the analytical calculation. If we assume that the bulk HTSs in the BHSAU are infinitely long in the x direction and that the BHSAU has an infinite periodic number, the magnetic field can be calculated under a two-dimensional approximation. Figure 2 shows the geometry used for the calculation. Here, D_y and D_z are the height and

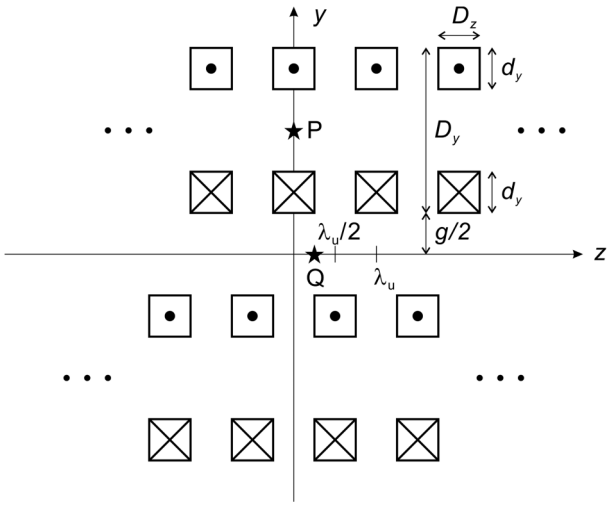

FIG. 2. Geometry used for analytical calculation.

thickness of the bulk, d_y is the depth of the layer to which the current penetrates, and the coordinates of points P and Q are $(z, y) = (0, (D_z + g)/2)$ and $(\lambda_u/4, 0)$, respectively. The centers of the bulk HTSs in the upper side are located at $z = n\lambda_u (n = \ldots, -1, 0, 1, \ldots)$ and those in the lower side are located at $z = (n + 1/2)\lambda_u (n = \ldots, -1, 0, 1, \ldots)$. The amplitude of the undulator field is equal to the y component of the field at point Q, i.e., $B_0 = B_y(\mathrm{Q})$. On the basis of Bean's critical state model of a type-II superconductor [23], we assumed the following. The loop current flows inside the bulk from its outer edge; the layer containing the flowing current has depth d_y. The current density at all points is equal to the average constant critical current density, J_c^{bulk}, over the entire bulk. The loop current inside the superconductor flows to negate the change in the solenoid field; therefore, the z-direction field at point P is equal to the change in the solenoid field after the superconducting transition, i.e., $B_z(\mathrm{P}) = -\Delta B_s$.

We next derive analytical formulas from the model. Using the two-dimensional Biot-Savart law, we have

$$B_0 = \mu_0 J_c^{\mathrm{bulk}} \lambda_u \sum_{n=1}^{\infty} \frac{\sin(nk_u D_z/2)}{n^2\pi^2} \times e^{-nk_u g/2}\left(1 - e^{-nk_u(D_y - d_y)}\right)\left(1 - e^{-nk_u d_y}\right) \quad (0 \le d_y < D_y/2), \tag{1}$$

$$\Delta B_s = -\frac{\mu_0 J_c^{\mathrm{bulk}}}{2}[d_y + T(\lambda_u, g, D_z, D_y, d_y)], \quad T/d_y < 10^{-3}. \tag{2}$$

Here, μ_0 is the vacuum permeability and k_u is the wave number of the undulator field, i.e., $k_u = 2\pi/\lambda_u$. Writing $D_z = \lambda_u/2$ and assuming $D_y \gg \lambda_u$, then, in practical units,

$$B_0 \sim 0.13 J_c^{\mathrm{bulk}} \lambda_u \exp\left(-\pi \frac{g}{\lambda_u}\right)\left[1-\exp\left(-\frac{4\pi \Delta B_s}{\mu_0 J_c^{\mathrm{bulk}} \lambda_u}\right)\right]. \tag{3}$$

Here, the units of J_c^{bulk} and λ_u are kA/mm and mm, respectively.

Next, we derive formulas to calculate the control curve of B_0. This is the ΔB_s-B_0 curve used to control B_0 for wavelength tuning once B_0 reaches the target value of the operation. From Bean's critical state model, if we decrease ΔB_s from the target value, current in the reverse direction starts to flow from the outer edge of the bulk. Defining $d_y^{\downarrow}$ as the depth of the layer containing the current flowing in the reverse direction, then the magnetic field is described by the superposition of the magnetic fields generated by the positive current (whose depth is d_y) and the negative current (whose depth is $d_y^{\downarrow}$):

$$B_0^{\downarrow}(d_y^{\downarrow}) = \begin{cases} B_0(J_c, d_y) - 2B_0(J_c, d_y^{\downarrow}) & (0 < d_y^{\downarrow} \le d_y) \\ -B_0(J_c, d_y^{\downarrow}) & (d_y < d_y^{\downarrow} \le D_y/2). \end{cases} \tag{4}$$

The formula for $\Delta B_s^{\downarrow}(d_y^{\downarrow})$ is identical. If we stop decreasing ΔB_s and start to increase it again, current with the same direction as the original current starts to flow from the outer edge of the bulk. Defining $d_y^{\uparrow}$ as the depth of the layer in which this current flows, then the magnetic field is described by the superposition of the magnetic fields generated by the positive current (whose depths are d_y and $d_y^{\uparrow}$) and the negative current (whose depth is $d_y^{\downarrow}$):

$$B_0^{\uparrow}(d_y^{\uparrow}) = \begin{cases} B_0^{\downarrow}(d_y^{\downarrow}) + 2B_0(J_c, d_y^{\uparrow}) & (0 \le d_y^{\uparrow} \le d_y^{\downarrow}) \\ B_0(J_c, d_y) & (d_y^{\downarrow} < d_y^{\uparrow} \le d_y) \\ B_0(J_c, d_y^{\uparrow}) & (d_y < d_y^{\uparrow} \le D_y/2). \end{cases} \tag{5}$$

The formula for $\Delta B_s^{\uparrow}(d_y^{\uparrow})$ is identical.

B. Numerical calculation

1. Three-dimensional model of bulk

In this study, the path of the loop current inside the bulk is fixed and spatially discretized. Figure 3 shows the three-dimensional model of the rectangular bulk (upper) and D-shaped bulk (lower) considered in this study. The rectangular bulk is used for the comparison of the two methods and the comparison with the analytical calculation. Because a sufficiently large D_x ($D_x = 10\lambda_u$) is assumed for the rectangular bulk, the calculation geometry is similar to that used in the two-dimensional analytical calculation ($D_x \to \infty$). Also, $D_y = 2\lambda_u$ is commonly used in the comparison between the analytical and numerical calculations. Here, from Eq. (1), the maximum B_0 when $D_y = 2\lambda_u$ is over 99% of that when $D_y \to \infty$. The D-shaped bulk has the same shape as the bulk used in the experiment ($R = 12.5$ mm) and is used for the comparison between the experiment and the numerical calculation. The left figures are cross-sectional views in the yz plane and the right figures are cross-sectional views in the xy plane. Here, N_z and N_y are the numbers of divisions of the bulks in the z and y directions, respectively. The stars indicate the center of the bulks. We assumed that the loop current flows only in the plane perpendicular to the z axis. This is because the z component is dominant in the solenoid field and in a field generated on a bulk HTS by other bulk HTSs. According to the assumption of Bean's critical state model for a type-II superconductor, the critical current density is constant throughout the bulk; thus, each loop has an equal current:

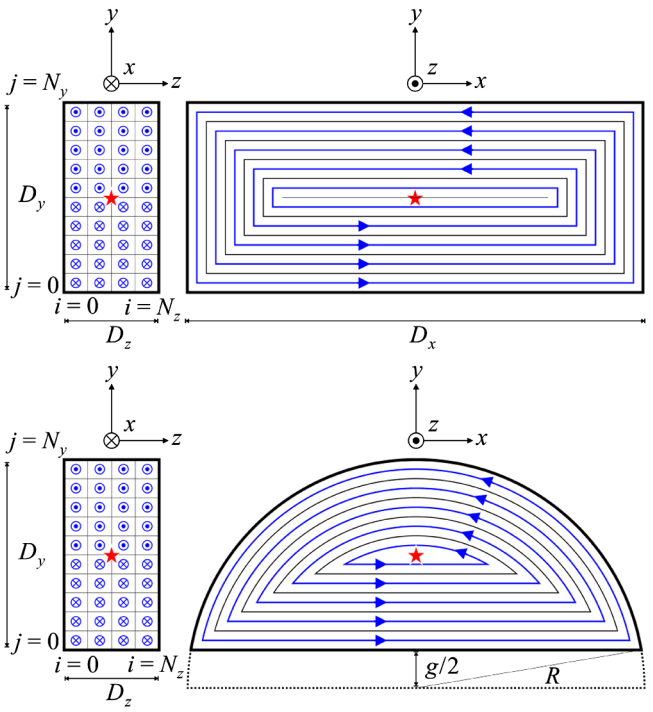

FIG. 3. Three-dimensional model of bulk HTS.

$$I_{ij} = I_c = J_c^{\mathrm{bulk}} \frac{D_z D_y}{2N_z N_y} (0 \le i < N_y, 0 \le j < N_z). \tag{6}$$

2. Center field method

The basic idea of the center field (CF) method is the same as that used in the analytical calculation. The loop current flows to negate the change in the solenoid field at the center of the bulk.

The key differences of this method from the analytical calculation are the finite periodic number and, for the D-shaped bulk, the three-dimensional geometry. Because of the finite periodic number, we assumed that each bulk HTS has a different depth at which the current flows, $d_{y,G}(G = 1, \ldots, 2N)$. Here, N is the periodic number of the undulator and $2N$ is the number of bulks. We also assumed that each depth is determined by the change in B_z at the center of each bulk HTS, $B_z(\mathbf{r}_{c,G})$. By defining $\mathbf{B}_{GH}$ as the magnetic field generated by the Hth bulk at the center of the Gth bulk, we obtained $B_z(\mathbf{r}_{c,G})$ as

$$B_z(\mathbf{r}_{c,G}) = \left[\sum_{H=1}^{2N} \mathbf{B}_{GH}(d_{y,H})\right]_z. \tag{7}$$

By using the above-mentioned assumption $B_z(\mathbf{r}_{c,G}) = -\Delta B_s$,

$$\left[\sum_{H=1}^{2N} \mathbf{B}_{GH}(d_{y,H})\right]_z + \Delta B_s = 0. \tag{8}$$

To determine all $d_{y,G}$, an iterative computation was performed.

In the computation, d_y is discretized by n_y. Here, n_y is the discretized depth of the layer in which the current flows ($0 \le n_y \le N_y$). Moreover, to obtain a high-precision result with a small number of divisions in the y direction (N_y), we assumed that the current I_c flowed in n_y lines and that a current of $\alpha I_c (0 \le \alpha < 1)$ flowed in the $(n_y + 1)$th line. Here, α is calculated from the residual $\Delta B_s - B_z(\mathbf{r}_{c,G})$ in each iteration. Then, the field at the center of the Gth bulk generated by loop ij in the Hth bulk is obtained using the discretized Biot-Savart law:

$$\mathbf{B}_{GHij} = \frac{\mu_0 I_c}{4\pi} \sum_{p=1}^{N_c} \frac{\Delta \mathbf{s}_p \times \mathbf{r}}{r^3}. \tag{9}$$

Here, N_c is number of the line elements (the number of divisions of the loop), $\Delta \mathbf{s}_p$ is the pth line element of loop ij in the Hth bulk, and r is the distance between $\mathbf{r}_{c,G}$ and the center of the line element. Then, the field $\mathbf{B}_{GH}$ is expressed by

$$\mathbf{B}_{GH}(n_{y,H}) = \sum_{i=1}^{N_z} \left(\sum_{j=1}^{n_{y,H}} B_{GHij} + \alpha B_{GHi(n_{y,H}+1)} \right). \tag{10}$$

3. Energy minimization method

The energy minimization (EM) method was proposed by Badía *et al.* to determine the critical state in which a system organizes itself [24]. Sanchez and Navau applied the method to a single bulk HTS with a finite height and cylindrical symmetry [25]. The shielding current distribution of a finite cylinder can be obtained with a constant J_c or field-dependent J_c under a uniform/nonuniform applied field.

In this study, to use the EM method for the three-dimensional problem of bulk HTSs with an arbitrary shape, we assumed the path of the loop current and used the discretized Neumann formula to compute the inductance.

The EM method is as follows. The energy required for the current to flow is the sum of the work required for the current to flow against the magnetic field induced by other loops and the energy obtained upon the vanishing of the external field. For current I_{ij} to flow in loop ij, the required energy is written as

$$\begin{aligned} E_{ij} &= I_{ij}(\Phi_{ij}^{\mathrm{int}} - \Phi_{ij}^{\mathrm{ext}}) \\ &= I_{ij}\left(\sum_{kl}^{N_y N_z} M_{ij,kl} I_{kl} - \int_{S_{ij}} B_{\mathrm{ext}} \mathrm{d}S \right). \end{aligned} \tag{11}$$

Here Φ_{ij}^{int} is the magnetic flux on the surface surrounded by loop ij generated by the other loops, Φ_{ij}^{ext} is the magnetic flux by the external field on the same surface, and $M_{ij,kl}$ is the mutual inductance ($ij \neq kl$) or self-inductance ($ij = kl$) between the loops. If a constant J_c is assumed, I_{ij} and I_{kl} are both equal to I_c. The calculation procedure is as follows: (1) Calculate E_{ij} for every loop that does not have a current. (2) Finish the calculation if there is no loop with $E_{ij} < 0$. (3) Find the loop with the minimum E_{ij}. (4) Flow a current in the loop. (5) Repeat the calculation from step (1). The current distribution after the calculation shows the critical state.

The model can be applied to three-dimensional problems with bulk HTSs of an arbitrary shape if the path of the loop current is determined in advance. We assumed the current path shown in Fig. 3 in common with that in the CF method. The current flows in a fixed plane normal to the z axis. This is similar to the thin-film approximation used in finite element analysis for bulk HTSs. However, in the thin-film approximation, the current path is free in the plane normal to the z axis; in this model, the current path is fixed in the plane to calculate the inductances in advance.

For a loop current with an arbitrary shape, it is difficult to find analytical formulas for the mutual inductance and self-inductance. Therefore, we numerically calculated the mutual inductance and self-inductance. The vector potential generated by loop kl at position $\mathbf{r}$ is described by the Biot-Savart law:

$$\mathbf{A}_{kl}(\mathbf{r}) = \frac{\mu_0 I_{kl}}{4\pi} \oint_{C_{kl}} \frac{\mathrm{d}\mathbf{s}_2}{r}. \tag{12}$$

Here I_{kl} is the current flowing in loop kl and C_{kl} is the integration path on the loop. The magnetic flux generated by loop kl on the surface surrounded by loop ij is expressed by

$$\Phi_{ij,kl} = \oint_{C_{ij}} \mathbf{A}_{kl} \cdot \mathrm{d}\mathbf{s}_1 = \frac{\mu_0 I_{kl}}{4\pi} \oint_{C_{ij}} \oint_{C_{kl}} \frac{\mathrm{d}\mathbf{s}_1 \cdot \mathrm{d}\mathbf{s}_2}{r}. \quad (13)$$

By discretizing the formula, we obtain the mutual inductance between loops ij and kl:

$$M_{ij,kl} = \frac{\Phi_{ij,kl}}{I_{kl}} = \frac{\mu_0}{4\pi} \sum_{p}^{N_c} \sum_{q}^{N_c} \frac{\Delta s_{ijp} \Delta s_{klq}}{r_{pq}}. \quad (14)$$

Here Δs_{ijp} and Δs_{klq} are respectively the pth and qth line elements of loops ij and kl, r_{pq} is the distance between the centers of the two elements, and N_c is the number of line elements (the number of divisions of the loop). The self-inductance of loop ij is calculated as the mutual inductance between loop ij and a slightly larger copy of loop ij, which is at a distance of $0.78 D_y/2/N_y$ from loop ij. For a torus with major radius R_{ij} and minor radius $D_y/2/N_y/2$, the calculation using this distance matches the analytical solution of the self-inductance. For a bulk HTS with an arbitrary shape, we define R_{ij} as the smallest distance in the y direction between loop ij and the center of the bulk HTS (the star in Fig. 3).

III. CALCULATION RESULTS AND COMPARISON WITH EXPERIMENT

A. Analytical results

Equation (3) shows that the BHSAU has a much higher undulator field than conventional undulators at a high critical current density. As examples, the maximum undulator fields obtained with three representative parameter sets are shown in Table II. One can obtain the maximum B_0, i.e., $B_{0,\max}$, by substituting the value of J_c listed in Table I. Here, parameter set (a) comprises values for the IVU in SACLA, (b) comprises those in our experimental setup, and (c) comprises those giving our target period.

Figure 4 shows the dependence of B_0 on ΔB_s at $\lambda_u =$ 10 mm and $g = 4$ mm. The upper figure shows the initial curves for various J_c^{bulk}. The plot was obtained from Eqs. (1) and (2) by using d_y as a parameter. The lower figure shows (1) the initial curve and sample control curves, i.e., (2) a curve to decrease B_0 and (3) a curve to increase B_0 again. The plot was obtained from Eqs. (4) and (5) using d_y,

TABLE II. Examples of maximum B_0 and ΔB_s (analytical).

	λ_u [mm]	g [mm]	$B_{0,\max}/J_c$ [T/kA/mm^2]	$\Delta B_{s,\max}/J_c$ [T/kA/mm^2]
(a)	18	3.6	1.26	13.4
(b)	10	4	0.364	7.45
(c)	5	1	0.350	3.72

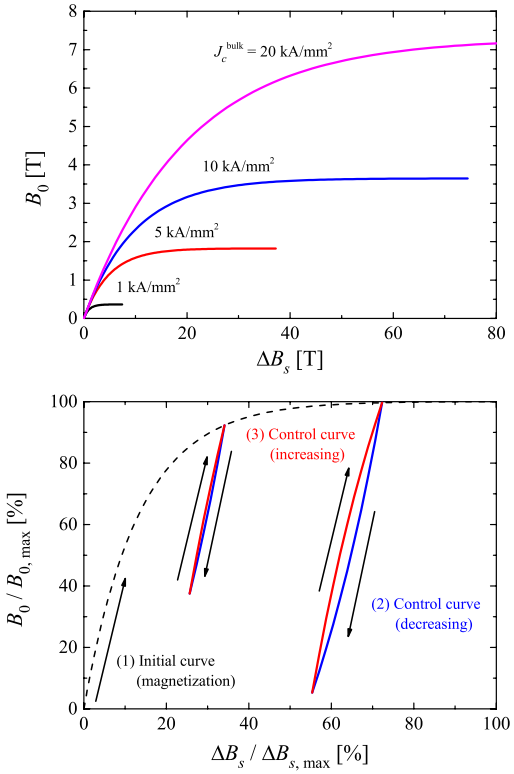

FIG. 4. Dependence of B_0 on ΔB_s (analytical, $\lambda_u = 10$ mm, $g = 4$ mm). The upper figure shows the initial curves for various J_c^{bulk}. The lower figure shows the initial curve and the sample control curves.

$d_y^{\downarrow}$, and $d_y^{\uparrow}$ as parameters. Here, the initial curve is the curve when the bulk is magnetized after the superconducting transition, and the control curves are the curves used to tune the wavelength of the undulator radiation during operation. There was hysteresis in the ΔB_s-B_0 curve.

Table III shows values of B_0 and the corresponding values of ΔB_s required to obtain each B_0. Here, Γ_y is defined as $\Gamma_y = 2d_y/D_y$ and is the depth of the field-penetrated layer in which the current flows. The values in this table have an error within 2% over a wide range of conditions ($0.1 \le g/\lambda_u \le 10$).

TABLE III. Examples of values of B_0 and the corresponding values of ΔB_s required to obtain each B_0 (analytical, $B_0/B_{0,\max}$ has an error of 2% in the range $0.1 \le g/\lambda_u \le 10$).

Γ_y [%]	$B_0/B_{0,\max}$ [%]	$\Delta B_s/\Delta B_{s,\max}$ [%]
5	29	4.2
10	48	8.5
15	63	12.7
20	72	17.0
25	80	21.2
30	86	25.5
100	100	100

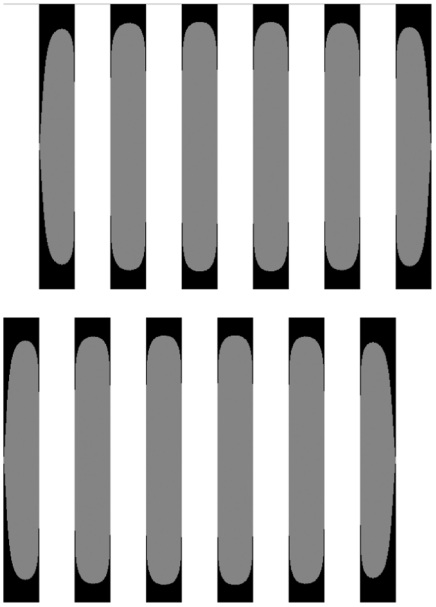

FIG. 5. Cross-sectional view of current distribution (EM method). The black area indicates where the current is flowing. The gray area indicates where the current is not flowing.

B. Numerical results

Figure 5 shows a cross-sectional view of the current distribution (x-direction current in zy plane) in the BHSAU with $N = 6$ obtained by the EM method. The black area indicates where the current is flowing and the gray area indicates where the current is not flowing. The depths of the layer in which the current flowed at the bulk edge and bulk center were markedly different, even in the bulk near the undulator center. The bulk HTSs at the end of the undulator showed an asymmetric distribution of the depths. The depth of the layer in which the current flowed in the single bulk was flat in the calculation by the CF method, as was expected from the assumption. However, without relation to the difference in the current distributions, the total amounts of the current in the bulk near the center had at most 1% difference between the CF and EM methods.

Figure 6 shows the dependence of B_0 on the parameter f, which is defined by $f = 1 - D_z/\lambda_u$: the ratio of the horizontal gap between two bulk HTSs to the period. The numerical calculation was performed by the CF and EM methods with $N = 12$. To compare the numerical and analytical results, the numerical (analytical) fields at various f were normalized by the numerical (analytical) value for $f = 0.5$. In the analytical calculation and the numerical calculation by the CF method, for both $f < 0.5$ and $f > 0.5$ almost the same degradation of B_0 was observed for all ΔB_s. In contrast, in the numerical calculation by the EM method, the $f > 0.5$ condition sometimes resulted in a higher B_0 than the $f = 0.5$ condition at low ΔB_s.

Figure 7 shows the difference in the analytical and numerical values of ΔB_s required for the same B_0. Here, the

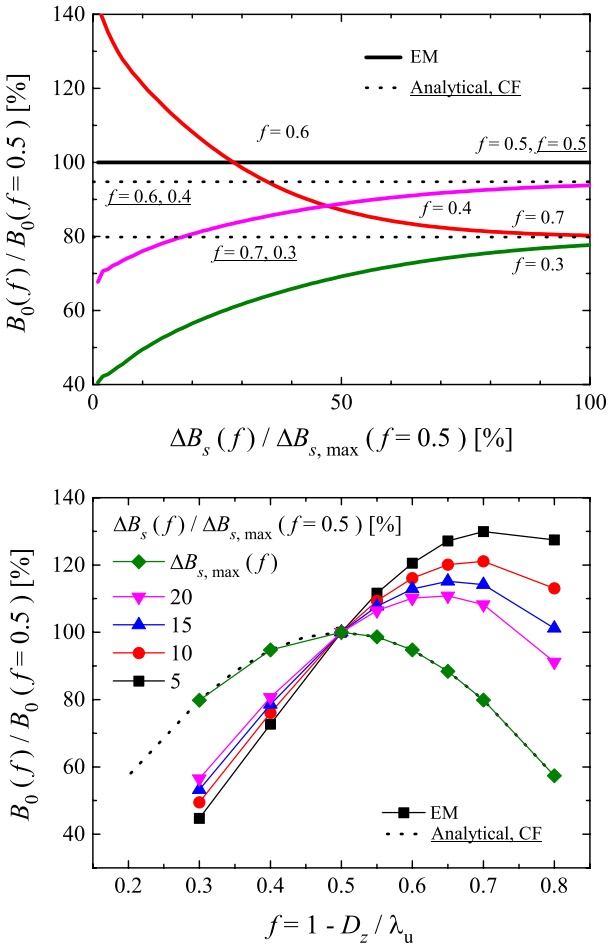

FIG. 6. Dependence of B_0 on f (analytical, CF, and EM, $g/\lambda_u = 0.4$). For comparison, the analytical (numerical) fields at various f are normalized by the analytical (numerical) value for $f = 0.5$.

superscripts An and Nu indicate analytical and numerical values, respectively. The numerical calculation was performed by the EM method with $N = 12$. B_0^{An} and ΔB_s^{An} are the values respectively obtained by Eqs. (1) and (2). In the numerical calculation, a larger ΔB_s than the analytical value was required to generate the same B_0, particularly for low B_0. For $f = 0.5$, the numerical value of ΔB_s required was up to 50% higher than the analytical value. For $f > 0.5$, the requirement was moderate at low B_0. The divergence at high B_0 for $f > 0.5$ means that $B_0(f)$ $(f > 0.5)$ cannot reach $B_{0,\max}(f = 0.5)$.

C. Comparison between experiment and calculation

The experiment was performed with a 6-periodic-number, 10-mm-period, 4-mm-gap prototype with a 2 T superconducting solenoid and a helium gas cooling system. To equalize the geometry, the calculation was performed with a D-shaped bulk with the same size as that used in the experiment, $f = 0.5$, $N = 6$, $\lambda_u = 10$ mm, and $g = 4$ mm.

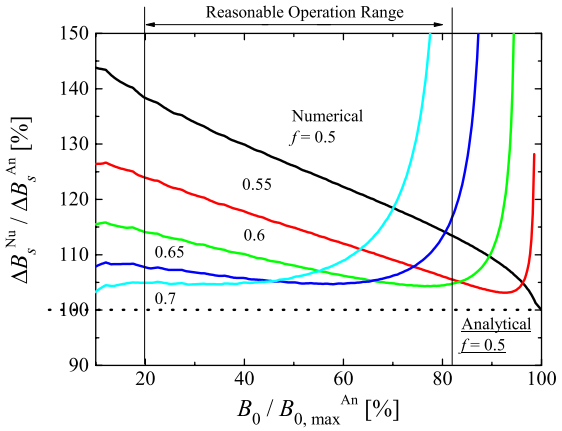

FIG. 7. Difference in the analytical and numerical values of ΔB_s required for the same B_0 (analytical and EM, $g/\lambda_u = 0.4$). The superscripts An and Nu indicate analytical and numerical values, respectively. The numerical calculation was performed by the EM method with $N = 12$.

The experimental results have an error of 4% owing to the measurement error. The setup of the experiment is described in Ref. [19].

Figure 8 shows a comparison of the experimental and calculated solenoid field dependences of the undulator field. The experimental results show data obtained at $T = 20$, 40, and 60 K. The calculation results show data obtained at $J_c = 10$, 5, 2, and 1 kA/mm^2. The green dotted lines indicate the results obtained by the CF method and the pink solid lines indicate the results obtained by the EM method. The initial gradients of the curves, $dB_0/d\Delta B_s|_{\Delta B_s=0}$ obtained by the experiment were 0.24 for all T, and those obtained by the EM and CF methods were 0.24 and 0.4, respectively, for all J_c^{bulk}.

Figure 9 shows a comparison of the experimental and calculated field distributions of B_y along the z axis. In the experiment, after the prototype was cooled to 20 K under a solenoid field of $B_s = -2$ T, the solenoid field was

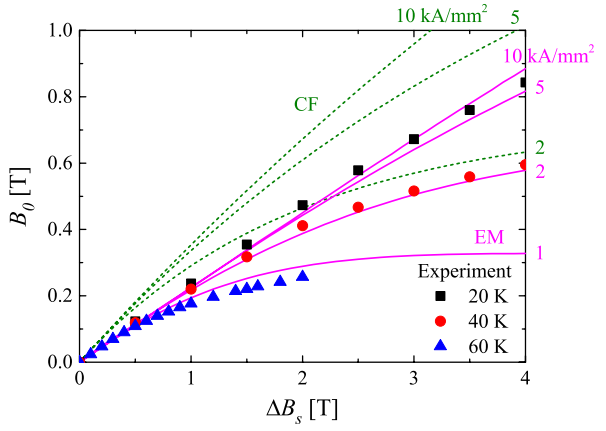

FIG. 8. Comparison of experiment and calculation: dependence of B_0 on ΔB_s.

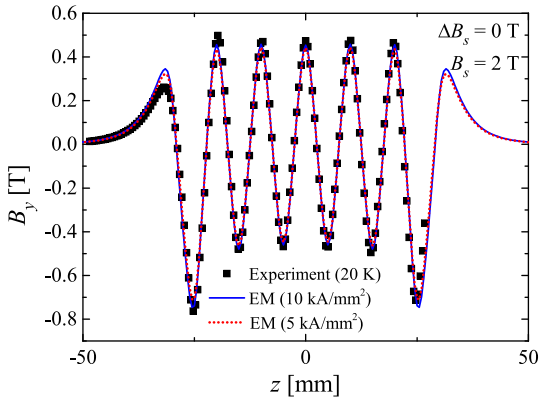

FIG. 9. Comparison of experiment and calculation: B_y distribution along the z axis.

changed to $B_s = 0$ T ($\Delta B_s = +2$ T) at $T = 20$ K. This is known as field cooling. The calculation was performed by the EM method with $J_c = 5$ and 10 kA/mm^2.

IV. DISCUSSION

A. Basic characteristics of fields

Here we clarify the characteristics of the BHSAU from the analytical calculations. Equation (1) shows that the undulator field of the BHSAU has common properties with that of a conventional Halbach-type PM undulator [20], such as the exponential dependence of the field on the gap and on the height of the magnet. Meanwhile, the undulator field of the BHSAU has the unique property that it depends on J_c^{bulk}, λ_u, and d_y. Equation (3) also shows that the BHSAU has a much higher undulator field than conventional undulators at a high J_c^{bulk}. Although its performance will be estimated later, here we introduce one example. If J_c is over 2 kA/mm^2, $B_{0,max}$ under condition (a) is twice as large as the peak field in the present IVU ($B_0 = 1.30$ T at $\lambda_u = 18$ mm, $g = 3.6$ mm). From Fig. 4, we obtain two findings. One is that the controllability of B_0 by the solenoid is maintained even in the saturation region in which B_0 is close to $B_{0,max}$. This is a feature different from a conventional SAU, which has little controllability in the saturation region, and is beneficial for tuning the wavelength. The other is that the ΔB_s required to obtain $B_{0,max}$ at a high J_c is greater than that for present commercially available solenoids. Fortunately, as shown in Table III, there is a "reasonable operation range" in which $\Delta B_s/\Delta B_{s,max}$ is much less than $B_0/B_{0,max}$. For example, almost half the value of $B_{0,max}$, $B_0/B_{0,max} = 48\%$ can be obtained even when $\Delta B_s/\Delta B_{s,max} = 8.5\%$. Thus, for high J_c, the undulator should be operated in the reasonable operation range.

B. Dependence on f

We next discuss the additional properties of the BHSAU obtained from the numerical calculation by the EM method

that were not observed in the analytical calculation and the numerical calculation by the CF method. One of the differences is the dependence of B_0 on f. As shown in Fig. 6, a higher B_0 was observed for $f > 0.5$ than when $f = 0.5$ for the same value of ΔB_s. Because the CF method and the analytical calculation did not exhibit this phenomenon, it is not due to the effect of the finite periodic number but to the current distribution inside the bulk HTSs shown in Fig. 5. Here we discuss this in detail. Currents with two different directions that are symmetric with respect to the z axis generate equal values of B_y on the z axis with opposite signs. When $f < 0.5$, the number of such pairs increases with increasing bulk thickness; therefore, B_0 decreases. However, currents with two different directions that are symmetric with respect to a certain point on the z axis generate the same B_y at the point. When $f > 0.5$, the numbers of such pairs decrease with decreasing bulk thickness; therefore, B_0 also decreases when $f > 0.5$, similarly to when $f < 0.5$. However, only in the EM method is there an effect that increases B_0 when $f > 0.5$. In the EM method, the depth of the layer in which the current flows is large at the edge of the bulk. If the position of the edge moves in the z direction to a point far from the field peak, the absolute field at the point decreases, although the B_y component increases in some cases. Therefore, in the EM method, B_0 increases or decreases depending on the current distribution at a certain ΔB_s when $f > 0.5$. This dependence on f is opposite that for a conventional SAU, in which the undulator field is high at $f < 0.5$ [26].

C. Effect of current distribution

Here we evaluate the agreement between the calculation and experiment. It is difficult to compare the B_y profile or B_0 at a single value of ΔB_s without the exact value of the average J_c in the experiment. Thus, we used the dependence curve of B_0 on ΔB_s. As is clear from Eqs. (1) and (2), and as shown in Fig. 4, the shape of the ΔB_s-B_0 curve and its initial gradient $\mathrm{d}B_0/\mathrm{d}\Delta B_s|_{\Delta B_s=0}$ do not depend on J_c but on the geometrical parameters. This was also true in the numerical calculation even when the depth of the layer in which the current flowed had a distribution in the z direction inside the bulk, as shown by the numerical ΔB_s-B_0 curve in Fig. 9. The only exception is the case that the current distribution at each different T had a different shape for an equal $\Delta B_s/\Delta B_{s,\max}$. This is caused when the shape of the J_c-B curve changes markedly with T. However, we know from the dc magnetization measurement that the shape of the J_c-B curve did not change markedly with T and also this effect did not appear in the initial gradient of the experimental ΔB_s-B_0 curve in Fig. 9. Thus, by comparing the initial gradient, we can discuss the agreement without knowing the exact value of J_c.

From the comparison between the calculation and experiment, we clearly found that the results obtained by the EM method showed agreement with those of the experiment. The initial gradients of the curves in the experiment and the EM method are identical, whereas the initial gradient in the CF method is 1.7 times larger than that in the experiment. Moreover, the dependence curve of B_0 on ΔB_s in the calculation by the EM method is similar to that in the experiment. From the comparison, we can estimate the range of the average J_c in the experiment. Because the average J_c changes with the field, it is difficult and meaningless to estimate the exact value to fit the curve. The estimated average ranges of J_c were 5–10 $\mathrm{kA/mm^2}$ at $T = 20$ K, 2–3 $\mathrm{kA/mm^2}$ at $T = 40$ K, and approximately 1 $\mathrm{kA/mm^2}$ at $T = 60$ K . These ranges are almost within the ranges from $J_c(B = 0)$ to $J_c(B = 2\mathrm{T})$ in Table I, and are thus thought to be reasonable. From these findings, we can conclude that the results of the EM method show agreement with those of the experiment. Additionally, we found that the macroscopic J_c in the bulk HTSs was almost equal to that of the small sample. This means that the large degradation due to the difficulty of manufacturing large bulk HTSs or cracking did not occur.

The reason for the agreement is next discussed. The geometrical parameters N, λ_u, g, D_x, D_y, and D_z and the bulk shape were equal in the experiment, the CF method, and the EM method. As stated in Sec. III A, the total amounts of current inside the bulk at the same ΔB_s are only slightly different for the two calculation methods. The only remaining factor is the geometrical shape of the current, i.e., the current distribution inside the bulk. Therefore, we conclude the following. The reason why the EM method closely reproduced the experiment is that it closely reproduced the current distribution in the experiment. The current distribution inside the bulk must be considered to precisely estimate the field inside the BHSAU.

We next discuss the results shown in Fig. 9. On the basis of the above discussion, the calculation was performed by the EM method with $J_c = 5$ and 10 $\mathrm{kA/mm^2}$. The difference between the results obtained experimentally and by calculation for both J_c is less than 5% except near the peak at $z \sim -32$ mm. By considering the fact that the measurement has an error of 4%, the difference of 5% is not large. The difference near the peak at $z \sim -32$ mm is about 30%. There are two possible reasons for this large difference. One is that the individual differences in J_c among the bulk HTSs particularly affect peaks near the ends of the undulator. The other is that the current distribution cannot be reproduced well near the ends of the undulator even by the EM method. The former effect can be included in the calculation by including the individual differences in J_c among the bulk HTSs. For the latter case, it is difficult to measure the actual current distribution inside the bulk HTSs. However, the difference can be evaluated by comparing a much larger amount of data, i.e., the B_y and B_z distributions in three-dimensional space near the ends of the undulator. If a difference appears, the assumption that

the current flows only in the plane perpendicular to the z axis should be changed in a future calculation.

Although the amplitude of the undulator field can be obtained by the empirical formulas derived in the next section, the numerical code remains useful for future research. As PMs have individual differences in magnetization, bulk HTSs also have differences in their critical current density, which cause the errors in the undulator field, such as so-called phase error and residual field integrals. Methods of compensating for these errors are practically important and the next topic of our research. It is not difficult to modify the numerical code to treat individual differences in the critical current density of bulk HTSs. Therefore, the numerical code can be used to study methods of compensating for these errors.

D. Empirical formulas

Next we modify the analytical formulas by using the results obtained by comparing the numerical and analytical calculations. The maximum B_0 in the numerical calculation is equal to that in the analytical calculation; therefore, the target range of the modification is the reasonable operation range discussed previously, and modification should be applied to the formula for ΔB_s but not to the formula for B_0:

$$B_0^{\mathrm{Nu}} = B_0^{\mathrm{An}}, \tag{15}$$

$$\Delta B_s^{\mathrm{Nu}} = (1+\alpha)\Delta B_s^{\mathrm{An}}. \tag{16}$$

As shown in Fig. 7, the factor α is at most 50%. However, if a suitable f is chosen for the target operation point, it can be less than 5%. We fit the curves by the empirical formula,

$$\alpha = a + b\frac{B_0^{\mathrm{An}}}{B_{0,\mathrm{max}}^{\mathrm{An}}} + c\exp\left(d\frac{B_0^{\mathrm{An}}}{B_{0,\mathrm{max}}^{\mathrm{An}}}\right) \quad (\text{for } a, b, c, \text{ and } d, \text{see}). \tag{17}$$

The fitting results of the parameters a, b, c, and d are shown in Table IV. The error of the formula is less than 1% in the effective range shown in Table IV.

Additionally, we consider the effect of the periodic number. Because we used $N = 12$ in the calculation for Fig. 7, the required ΔB_s should be modified as

$$\Delta B_s^{\mathrm{Nu}}(N) = \beta(N) \times (1+\alpha)\Delta B_s^{\mathrm{An}}. \tag{18}$$

Here, β is a function of the periodic number, and the right term of the multiplication is the value when $N = 12$. By fitting the dependence curve of ΔB_s on N for $B_0/B_{0,\mathrm{max}}^{\mathrm{An}} = 50\%$, we have

TABLE IV. Parameters for Eq. (17).

	$a + bx + c\exp(dx)$				
f	a	b	c	d	Effective range $B_0/B_{0,\mathrm{max}}$ [%]
0.55	0.296	−0.294	⋯	⋯	20–90
0.60	0.176	−0.188	7.93×10^{-9}	18.2	20–90
0.65	0.0995	−0.107	1.50×10^{-5}	11.2	20–80
0.70	0.0551	−0.0346	1.47×10^{-4}	9.89	20–70

$$\beta(N) = 1.098 - 1.060\frac{1}{N} - 1.519\frac{1}{N^2}. \tag{19}$$

The error of this formula is less than 1% in the range of $N \geq 6$ and $20 \leq B_0/B_{0,\mathrm{max}}^{\mathrm{An}} \leq 90$.

Equation (18) reproduces the numerical B_0 and ΔB_s with an error of less than 2% for $D_y = 2\lambda_u$, $g/\lambda_u = 0.4$, $N \geq 6$, and the effective $B_0/B_{0,\mathrm{max}}$ range shown in Table IV. Moreover, because it is clear from Table III that the shape of the ΔB_s-B_0 curve has a difference of less than 2% among various values of g/λ_u, this modified formula can be applied to a wide range of conditions ($0.1 \leq g/\lambda_u \leq 10$) with an error of less than 3%.

E. Usage of formulas and performance estimation

Here we estimate the magnetic performance of the BHSAU as an example of using the formulas and the values obtained above. As examples of performance estimation, we calculated two patterns with $\lambda_u = 18$ mm and $g = 3.6$ mm by targeting a field twice as large as that generated in the IVU but with an equal period and gap. Next, we calculated two patterns with $\lambda_u = 10$ mm and $g = 4$ mm by targeting $K = 2$ and two patterns with $\lambda_u = 5$ mm and $g = 1$ mm by targeting $K = 1$ and 2. Here, K is called the deflection parameter and is defined by $K = eB_0\lambda_u/(2\pi mc)$, where e and m are the electron charge and mass, respectively. To obtain bright undulator radiation, $K \sim 1$–2 is required.

In Table V, we show the estimated B_0, and the values of ΔB_s and the operation temperature T required to obtain each B_0. Here, ΔB_s is the value for $N = 50$. Note that Γ_y is not the actual depth of the layer in which the current flows and is simply the index in Table III. We set J_c^{bulk}, Γ_y, f, and

TABLE V. Performances of BHSAU.

λ_u [mm]	g [mm]	J_c^{bulk} [kA/mm^2]	Γ_y [%]	f	B_0 [T]	$\Delta B_s/2$ [T]	T [K]	K
18	3.6	2.4	30	0.6	2.6	4.8	40	4.4
		7.1	5	0.7	2.6	2.3	20	4.4
10	4	8.0	20	0.6	2.1	6.0	20	2.0
		12.0	10	0.65	2.1	4.4	10	2.0
5	1	7.1	30	0.6	2.1	3.9	20	1.0
		16.7	20	0.6	4.2	6.0	4	2.0

T to satisfy the following conditions: (i) $\Delta B_s/2$ does not exceed 6 T, (ii) J_c^{bulk} is in the range from $J_c(B=0)$ to $J_c(B=\Delta B_s/2)$ at T, (iii) f is chosen to obtain a small α. Here, we assumed the field cooling method, i.e., the undulator is cooled to below the superconducting transition temperature under a solenoid field of $-\Delta B_s/2$ and operated under a solenoid field of $\Delta B_s/2$. Thus, we used J_c^{bulk} in the range between $J_c(B=0)$ and $J_c(B=\Delta B_s/2)$.

As shown in the table, an undulator field twice as large as that of the present IVU but with an equal period and gap can be obtained at temperatures of approximately 20–40 K. Moreover, $K=1$ or 2 can be achieved with a short period such as 5 or 10 mm. Because B_0 of over 4 T is required to achieve $K=2$ at $\lambda_u=5$ mm, it is impossible to achieve this using PM undulators even with $g=0$. Although $T=4$ K is required to achieve the condition of the bottom row in Table V with currently available bulk HTSs, if the critical current density of the bulk HTS is doubled as a result of future material developments, the BHSAU can be operated at approximately 20 K. We believe that the magnetic field strength of the BHSAU is sufficiently high for future high-field short-period undulators.

V. CONCLUSION

The magnetic field inside a BHSAU was calculated by analytical and numerical methods to reveal its characteristics. The analytical calculation showed that a high undulator field could be achieved by the BHSAU at a high critical current density and that good undulator field tunability was maintained even in the saturation region. The numerical calculation by the EM method, which treats the current distribution inside the bulk HTSs, produced a considerably different current distribution from that obtained by the CF method, and closely reproduced the experimental results. Thus, we found that consideration of the current distribution is extremely important in calculating the undulator field and the required change in the solenoid field. To precisely estimate the fields without a large computation cost, by comparison between the analytical and numerical calculations, we obtained a semiempirical formula for the required solenoid field by modifying the analytical formula so that it treats the effect of the current distribution inside bulk HTSs. Finally, we estimated the magnetic performance of the BHSAU as an example of using the formulas and the values obtained in the discussion. The estimation showed that an undulator field twice as large as that of the present IVU but with an equal period and gap can be obtained at a temperature of approximately 20–40 K, and that $K=1$ and 2 can be achieved with $\lambda_u=5$ and 10 mm at approximately 4–20 K. We consider that the magnetic field strength of the BHSAU is sufficiently high for future high-field short-period undulators.

ACKNOWLEDGMENTS

This work was supported by MEXT KAKENHI Grant No. 21340057 and a Grant-in-Aid for JSPS Fellows, Grant No. 10J03477.

[1] P. M. Stefan, T. Tanabe, S. Krinsky, G. Rakowsky, L. Solomon, and H. Kitamura, J. Synchrotron Radiat. **5**, 417 (1998).
[2] T. Schmidt, G. Ingold, A. Imhof, B. D. Patterson, L. Patthey, C. Quitmann, C. Schulze-Briese, and R. Abela, Nucl. Instrum. Methods Phys. Res., Sect. A **467**, 126 (2001).
[3] J. A. Clarke, in *Proceedings of the European Particle Accelerator Conference, Vienna, Austria, 2000*, p. 2319.
[4] O. Chubar, C. Benabderrahmane, M. P. Level, O. Marcouille, and M. Massal, in *Proceedings of the 9th European Particle Accelerator Conference, Lucerne, 2004* (EPS-AG, Lucerne, 2004), p. 369.
[5] P. Emma *et al.*, Nat. Photonics **4**, 641 (2010).
[6] M. Hoener *et al.*, Phys. Rev. Lett. **104**, 253002 (2010).
[7] T. Ishikawa *et al.*, Nat. Photonics **6**, 540 (2012).
[8] J. Dai, H. Deng, and Z. Dai, Phys. Rev. Lett. **108**, 034802 (2012).
[9] D. J. Scott, J. A. Clarke, D. E. Baynham, V. Bayliss, T. Bradshaw, G. Burton, A. Brummitt, S. Carr, A. Lintern, J. Rochford, O. Taylor, and Y. Ivanyushenkov, Phys. Rev. Lett. **107**, 174803 (2011).
[10] H. Kitamura, J. Synchrotron Radiat. **7**, 121 (2000).
[11] T. Hara, T. Tanaka, H. Kitamura, T. Bizen, X. Maréchal, T. Seike, T. Kohda, and Y. Matsuura, Phys. Rev. ST Accel. Beams **7**, 050702 (2004).
[12] T. Hezel, B. Krevet, H. O. Moser, J. A. Rossmanith, R. Rossmanith, and T. Schneider, J. Synchrotron Radiat. **5**, 448 (1998).
[13] M. Tomita and M. Murakami, Nature (London) **421**, 517 (2003).
[14] T. Tanaka, T. Hara, H. Kitamura, R. Tsuru, T. Bizen, X. Marechal, and T. Seike, Phys. Rev. ST Accel. Beams **7**, 090704 (2004).
[15] T. Tanaka, R. Tsuru, and H. Kitamura, J. Synchrotron Radiat. **12**, 442 (2005).
[16] T. Tanaka, T. Hara, R. Tsuru, D. Iwaki, T. Bizen, X. Marechal, T. Seike, and H. Kitamura, Supercond. Sci. Technol. **19**, S438 (2006).
[17] R. Kinjo, T. Kii, H. Zen, K. Higashimura, K. Masuda, K. Nagasaki, and H. Ohgaki, in *Proceedings of the 30th International Free Electron Laser Conference, Geongju, Korea, 2008*, p. 473.
[18] A. H. Ho, R. H. Pantell, J. Feinstein, and B. Tice, Nucl. Instrum. Methods Phys. Res., Sect. A **296**, 631 (1990).
[19] R. Kinjo, M. Shibata, T. Kii, H. Zen, K. Masuda, K. Nagasaki, and H. Ohgaki, Appl. Phys. Express **6**, 042701 (2013).
[20] K. Halbach, Nucl. Instrum. Methods Phys. Res. **187**, 109 (1981).
[21] O. Chubar, P. Elleaume, and J. Chavanne, J. Synchrotron Radiat. **5**, 481 (1998).

[22] M. Morita, E. Teshima, and H. Hirano, Nippon Steel Corporation Technical Report No. 93, 2006.
[23] C. P. Bean, Rev. Mod. Phys. **36**, 31 (1964).
[24] A. Badía, C. López, and J. L. Giordano, Phys. Rev. B **58**, 9440 (1998).
[25] A. Sanchez and C. Navau, Phys. Rev. B **64**, 214506 (2001).
[26] J. Kitagaki, K. Masuda, Z. W. Dong, T. Kii, T. Yamazaki, and K. Yoshikawa, Nucl. Instrum. Methods Phys. Res., Sect. A **475**, 613 (2001).